straints is lessened, we expect that β would increase in the direction of unity, which is qualitatively consistent with the dependence on temperature observed in these experiments. This would lead ultimately to exponential relaxation, $\beta = 1$ (*9*).

Long-lived nonequilibrium states thus can result from steric pinning of molecules to the adsorbing surface; they need not reflect strong adsorption to that surface. The ensuing dynamical evolution of the surface composition displays a phenomenology analogous to the forms of complex dynamics that are well known for conventional glasses. The dynamic constraints on desorption can actually give rise to a divergence of the effective relaxation time; the temperature at which this occurs is expected to depend on the strength of segment-surface adsorption and on the density of pinning. Further work in which the polymer molecular weights are varied shows that displacement is more rapid when the chain length of the weakly adsorbing species is less (*17*) but remains nonexponential. The physical model suggested here may also have a bearing on interpreting dynamic aspects of flexible proteins at surfaces.

REFERENCES AND NOTES

1. P.-G. de Gennes, *Adv. Colloid Interface Sci.* **27**, 189 (1987).
2. M. A. Cohen-Stuart, T. Cosgrove, B. Vincent, *ibid.* **24**, 143 (1986).
3. A. Takahashi and M. Kawaguchi, *Adv. Polym. Sci.* **46**, 1 (1982).
4. I. Lundström, B. Ivarsson, U. Jönsson, H. Elwing, in *Polymer Surfaces and Interfaces*, W. J. Feast and H. S. Munro, Eds. (Wiley, New York, 1987), pp. 201–230.
5. W. Norde, *Adv. Colloid Interface Sci.* **25**, 267 (1986).
6. E. Pefferkorn, A. Carroy, R. Varoqui, *J. Polym. Sci. Polym. Phys. Ed.* **23**, 1997 (1985).
7. E. Pefferkorn, A. Haouam, R. Varoqui, *ibid.* **22**, 2677 (1989).
8. H. E. Johnson and S. Granick, *Macromolecules* **23**, 3367 (1990).
9. P. Frantz and S. Granick, *Phys. Rev. Lett.* **66**, 899 (1991).
10. M. A. Cohen-Stuart, G. J. Fleer, J. M. H. M. Scheutjens, *J. Colloid Interface Sci.* **97**, 515 (1984).
11. B. J. Fontana and J. R. Thomas, *J. Phys. Chem.* **65**, 480 (1961).
12. P.-G. de Gennes, *New Trends in Physics and Physical Chemistry of Polymers*, L.-H. Lee, Ed. (Plenum, New York, 1989), pp. 9–18.
13. P. M. Adriani and A. K. Chakraborty, *Macromolecules*, in press.
14. A. Chakraborty, J. S. Shaffer, P. M. Adriani, *ibid.* **24**, 5226 (1991).
15. For reviews of molecular motion in glass-forming systems, see G. Williams, *J. Non-Crystalline Solids* **131–133**, 1 (1991); G. H. Fredrickson, *Annu. Rev. Phys. Chem.* **39**, 149 (1988).
16. J. B. Hubbard, T. Nguyen, D. Bentz, *J. Chem. Phys.*, in press.
17. C. Thies, *J. Phys. Chem.* **70**, 3783 (1966).

18. We thank A. Chakraborty, J. Douglas, P.-G. de Gennes, J. Hubbard, M. Muthukumar, and K. Schweizer for discussions. Supported by National Science Foundation (Polymers Program) grant DMR-91-01509.

22 October 1991; accepted 6 January 1992

The Conformation of Fluid Membranes: Monte Carlo Simulations

D. M. KROLL* AND G. GOMPPER

The conformation and scaling properties of self-avoiding fluid membranes with an extrinsic bending rigidity κ were studied with the use of Monte Carlo methods. For $\kappa = 0$, the results are consistent with branched polymer behavior at large length scales. There is a smooth crossover from a crumpled to an extended state with increasing κ, with a peak in the specific heat when the persistence length reaches the system size. The scale-dependent effective bending rigidity is a decreasing function of system size for all bare rigidities. These results indicate that fluid membranes are always crumpled at sufficiently long length scales.

MEMBRANES COMPOSED OF AMphiphilic molecules, such as the monolayers of surfactant molecules at oil-water interfaces in microemulsions, the lipid bilayers that form biological membranes, as well as the layers of surfactant molecules in recently studied lyotropic liquid crystals, are highly flexible (nearly tensionless) surfaces. Membranes play a central role in determining the architecture of biological systems and provide the basic structural element for complex fluids such as microemulsions; an understanding of the statistical mechanics of these self-avoiding surfaces is therefore of considerable importance (*1, 2*).

In most cases of interest, these membranes are fluid, which means that the molecules can diffuse rapidly within the membrane surface and possess no reference lattice. In the absence of a lateral tension (*3, 4*), the shape of the membrane is governed by its bending rigidity κ. A membrane of linear size L exhibits transverse fluctuations (*5*) of extension $L_\perp \sim (kT/\kappa)^{1/2}L$ (where k is Boltzmann's constant and T is temperature) on length scales small compared to the persistence length (*6*) $\xi_p \equiv a \exp(c\kappa/kT)$, where a is a short-distance cutoff and $c = 4\pi/3$ (*7, 8*). However, as L approaches ξ_p, shape fluctuations have been predicted (*7, 8*) to reduce the bending rigidity and lead to a renormalized rigidity $\kappa_R = \kappa - (kT/c)\ln(L/a)$ in the limit of small kT/κ. On length scales $L \approx \xi_p$, the membrane should have an effective bending rigidity of the order of kT. At larger length scales ($L >> \xi_p$), membranes fluctuating at constant area are expected to have an extremely small bending rigidity and behave as crumpled (*9*) objects characterized by the absence of long-range orientational order of normals erected perpendicular to the local surface elements. For a fixed topology, the scaling behavior of self-avoiding fluid membranes at these length scales is expected to be the same as that of a branched polymer (*2, 10, 11*).

Several aspects of this scenario have, however, not yet been verified. Indeed, there is little evidence that self-avoiding fluid membranes with a finite bare bending rigidity really do crumple. It has been speculated (*2*) that self-avoidance may stabilize the effective bending rigidity at some finite value $\kappa \sim kT$ and therefore prevent crumpling. Furthermore, there is some controversy concerning the universality classes of the various models used to describe self-avoiding random surfaces (with $\kappa = 0$). The most widely studied models for these surfaces are constructed by taking the elementary 2-cells (plaquettes) on a hypercubic lattice and gluing them together in such a way that each edge is shared by exactly two plaquettes (*10*). For fixed topology, the long–length-scale behavior of this class of surface has been shown to be that of a branched polymer: the radius of gyration R_g of a surface of area S scales as $R_g^2 \sim S^\nu$ (*12*), with $\nu = 1$ in spatial dimension $d = 3$ (*10*). Recently, however, randomly triangulated surfaces of the type we consider here have been investigated for $\kappa = 0$ with the use of Monte Carlo techniques (*13*). A value $\nu \approx 0.8$ was reported, implying that such surfaces belong to a different universality class. Given the generality of the entropic mechanism behind branched polymer behavior, this discrepancy is troubling (*10, 11*).

In this report we present evidence that fluid membranes are crumpled at sufficiently large length scales for any value of the bare bending rigidity and that the crumpled state does indeed exhibit branched polymer behavior. Our conclusions are based on exten-

D. M. Kroll, AHPCRC, University of Minnesota, Minneapolis, MN 55415.
G. Gompper, Sektion Physik der Ludwig-Maximilians-Universität München, 8000 München 2, Germany.

*Permanent address: Institut für Festkörperforschung, KFA Jülich, 5170 Jülich, Germany.

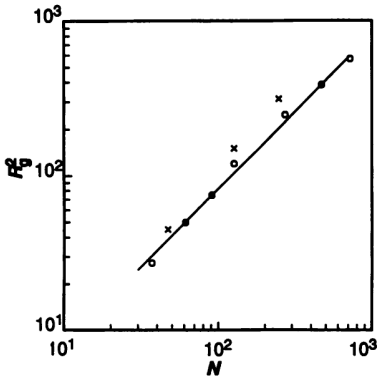

Fig. 1. Mean-squared radius of gyration R_g^2 versus the number of monomers N for $\lambda = 0$: (○) open membrane, $\ell_0^2 = 2.0$, free-edge boundary condition; and (×) vesicle, $\ell_0^2 = 2.8$. The solid line is a plot of $R_g^2 \sim N$.

sive simulations of a simple molecular model for self-avoiding fluid membranes for a wide range of bare bending rigidities. The simulations were carried out with a simple string-and-bead model for randomly triangulated two-dimensional surfaces embedded in three dimensions (*13–17*). Both planar (with free-edge boundary conditions) and spherical (vesicle) topologies were considered. In both cases the surface is modeled by a triangular network of N hard-sphere particles of diameter $\sigma = 1$. The energy assigned to a particular configuration is

$$\beta\mathcal{H} = -\lambda \sum_{\langle\alpha,\gamma\rangle} (\mathbf{n}_\alpha \cdot \mathbf{n}_\gamma - 1) + \sum_{\langle i,j\rangle} V_t(|\mathbf{r}_i - \mathbf{r}_j|) + \sum_{i>j} V_{HC}(|\mathbf{r}_i - \mathbf{r}_j|) \quad (1)$$

where $\beta = 1/kT$. In Eq. 1, the first sum runs over pairs $\langle\alpha,\gamma\rangle$ of unit vectors $\{\mathbf{n}_\alpha\}$ erected perpendicular to each elementary triangle in the lattice. The second summation is over neighboring pairs $\langle i,j\rangle$ of atoms (located at $\mathbf{r}_i$ and $\mathbf{r}_j$) in the array interacting through a tethering potential $V_t(r)$ that vanishes for $0 < r < \ell_0$ and is infinite otherwise. Finally, the third summation is over all pairs of atoms interacting through a repulsive hard core potential $V_{HC}(r)$ that vanishes for $r > 1$ and is infinite otherwise. Self-avoidance is enforced by choosing an $\ell_0 < \ell_0^{max}$; the value of ℓ_0^{max} depends on the updating procedure that is implemented (see below). The continuum limit of the bending energy term in Eq. 1 can be shown to be

$$F_b = \frac{1}{2}\kappa \int dS\,(H^2 - 2K) \quad (2)$$

where dS denotes the surface element and F_b is just Helfrich's curvature elastic energy with bending rigidity $\kappa = \lambda/\sqrt{3}$ (*18, 19*) and Gaussian rigidity $\kappa_G = -\kappa$; $H = c_1 + c_2$ and $K = c_1c_2$, where c_1 and c_2 are the principal curvatures.

Our Monte Carlo updating procedure consists of two steps: First, we attempt to sequentially update the position vector of each monomer by a random increment in the cube $[-s,s]^3$, where s is a constant to be chosen below. The probabilistic decision whether to accept the move is made by comparing the initial and final energies of the system. We chose s so that ~50% of the updating attempts were accepted. Second, we attempt to flip N randomly chosen bonds. A bond flip consists of deleting a tether and constructing a new one between the two previously unconnected vertices of the two adjacent triangles. The flip is accepted with the probability given by the Boltzmann factor if all vertices have a minimum of three neighbors (*20*). Note that this procedure does not flip boundary tethers, so that the open membranes we simulate have perimeters of constant length. A more detailed discussion of the bond-flipping procedure can be found in (*13–17*).

In order to insure reparametization invariance we use a discretized version of the invariant measure $\int D[\mathbf{r}] = \Pi_\xi [\int d\mathbf{r}(\xi) g^{3/4}(\xi)]$ in our simulations, where $\mathbf{r}(\xi)$ is the three-dimensional coordinate vector of a point on the surface with internal coordinate ξ and g is determinant of the metric tensor (*21*). We also choose a metric in which all internal lengths are equal, that is, all triangles on the surface are equilateral and of area one so that the volume ω_i of the dual image of vertex i (which is the discrete analog of the invariant volume $\int d^2\xi\sqrt{g}$) is proportional to the coordination number q_i of this vertex: $\omega_i = q_i/3$. On the triangulated surface the curvature is concentrated at the vertices; with the present normalization the scalar curvature $R_i = \pi(6 - q_i)/q_i$ and the discretization of the measure is $\Pi_i\, d\mathbf{r}_i\, \omega_i^{3/2}$ (*14–17*).

Simulations were performed with both $\ell_0 = \sqrt{2.0}$ and $\sqrt{2.8}$. In the former case we chose $s = 0.1$ and in the latter $s = 0.15$. This choice of parameters ensures self-avoidance when updating the monomer coordinates. However, there is only weak self-avoidance during bond flipping for $\ell_0 = \sqrt{2.8}$. Indeed, it is easy to show that implementing complete self-avoidance would require taking ℓ_0 at least less than $\sqrt{8/3}$ in this case. We have in fact observed vesicle inversion for $\ell_0 = \sqrt{2.8}$ when $\lambda = 0$. Nevertheless, data for the mean-squared radius of gyration R_g^2 for zero bending energy indicate that this does not influence the asymptotic fractal dimension of the crumpled phase. Furthermore, it does not qualitatively affect the behavior for finite λ. The primary advantage of using a larger tethering length is that the diffusivity of the monomers in the membrane surface is substantially enhanced: the bond-flip acceptance rate is a factor of 2 greater for $\ell_0 = \sqrt{2.8}$ than for $\sqrt{2.0}$ when $\lambda = 0$; the effect is greater for larger values of λ.

In Fig. 1 we plot data for R_g^2 versus the number of monomers for the case of zero bending rigidity, $\lambda = 0$. Averages were taken over 1×10^7 to 2×10^7 Monte Carlo steps per monomer. Data are shown both for vesicles with $\ell_0 = \sqrt{2.8}$ and planar membranes with $\ell_0 = \sqrt{2.0}$. For both topologies, the data are consistent with $R_g^2 \sim N^\nu$ (*12*) with $\nu = 1$. Furthermore, typical configurations, such as the one illustrated in Fig. 2, indicate a "branched polymer" structure in which there are long arms extending out in various directions. This result suggests an entropic mechanism that favors treelike ramified objects, which is in agreement with results obtained for random surfaces constructed of elementary plaquettes on a cubic lattice (*10*). For vesicles, our results are consistent with $S \sim R_g^2$ and $V \sim R_g^2$ (where S and V are the surface area and

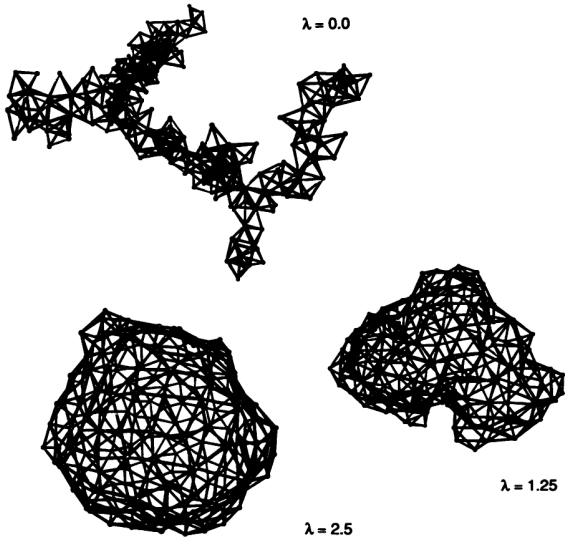

Fig. 2. Typical configurations of a vesicle with $N = 247$ monomers and $\ell_0 = \sqrt{2.8}$ for $\lambda = 0$, 1.25, and 2.5.

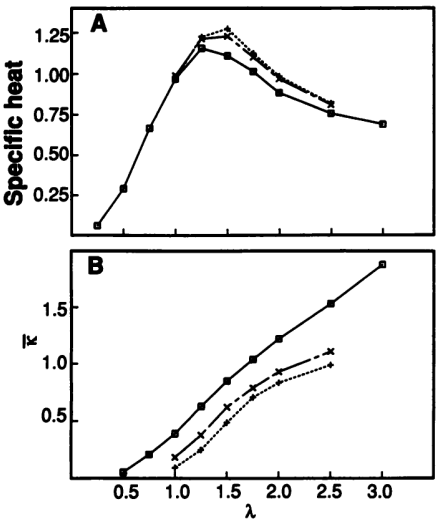

Fig. 3. (**A**) Specific heat obtained by using Eq. 3 for vesicles with $\ell_0 = \sqrt{2.8}$ and N = (□) 47, (×) 127, and (+) 247 monomers. (**B**) Effective bending rigidity $\bar{\kappa} = \kappa_{eff}/6$ obtained by averaging over $N_s = (N - 1)/2$ contiguous monomers on the vesicle surface by using Eq. 5.

volume enclosed by the vesicle).

Fluctuations are suppressed for finite λ, and as seen in Fig. 2, there appears to be a crossover from crumpled behavior for $\lambda << 1$ to a rough but extended phase for $\lambda >> 1$. Further evidence for this freezing out of degrees of freedom is given by the behavior of the specific heat per monomer

$$C \equiv \frac{\lambda^2}{N}[\langle E^2\rangle - \langle E\rangle^2] \qquad (3)$$

where $E = \Sigma_{\langle\alpha,\beta\rangle}\, \mathbf{n}_\alpha \cdot \mathbf{n}_\beta$. A plot of data obtained for vesicles with $\ell_0 = \sqrt{2.8}$ containing N = 47, 127, and 247 monomers (Fig. 3A) shows that there is a pronounced peak near $\lambda_c \approx 1.25$. Such a peak could signal the existence of a phase transition between a crumpled phase for low bending rigidities and a flat phase for large ones. In fact, it is argued in (*17*) that such a transition does indeed occur in membranes without self-avoidance. However, the height of the peak increases only slowly with N. This result implies that the specific heat exponent α must be very small (if there is a transition) or that the correlation length exponent ν must be quite large. In addition, the peak shifts to larger values of λ with increasing system size, which is the opposite of what is usually observed for finite size effects in systems with periodic boundary conditions. We believe the most plausible explanation is that the peak occurs when the persistence length ξ_p reaches the system size and that there is no phase transition.

An additional confirmation of this interpretation is given by the behavior of the scale-dependent effective bending rigidity κ_{eff}. The renormalized bending rigidity can be expressed in terms of the mean curvature susceptibility as (*22*)

$$\langle A\rangle/\kappa_{eff} = \int d^2\xi \sqrt{g(\xi)} \int d^2\xi' \sqrt{g(\xi')}\, \langle H(\xi)H(\xi')\rangle_c \qquad (4)$$

where $\langle A\rangle$ is the average membrane area, $\langle\cdots\rangle_c$ denotes the cumulant average, and $H(\xi)$ is the mean curvature at ξ. In the continuum limit, the extrinsic curvature tensor is proportional to the unit normal vector. The discretization (*23*) of $\int d^2\xi\sqrt{g(\xi)}H(\xi)$ we use is therefore $\Sigma_i s_i |\Sigma_{j(i)}(\sigma_{ij}/l_{ij})(\mathbf{r}_i - \mathbf{r}_j)|$, where the i-sum runs over monomers, the $j(i)$-sum runs over the neighbors of i, and s_i is the sign of $\hat{\mathbf{n}}_i \cdot \Sigma_{j(i)}(\mathbf{r}_i - \mathbf{r}_j)$, with $\hat{\mathbf{n}}_i$ the surface normal at monomer i obtained by averaging over the normals of all triangles that have i as a corner; l_{ij} is the distance between the two neighboring monomers i, j, and σ_{ij} is the length of a bond in the dual lattice. For the metric we have chosen, $\sigma_{ij}/l_{ij} = 1/\sqrt{3}$ so that the right-hand side of Eq. 4 becomes

$$\frac{1}{3}\left\langle \sum_i s_i \left| \sum_{j(i)} (\mathbf{r}_i - \mathbf{r}_j) \right| \sum_k s_k \left| \sum_{m(k)} (\mathbf{r}_k - \mathbf{r}_m) \right| \right\rangle_c \qquad (5)$$

For vesicles, the amplitude of the average in Eq. 4 depends strongly on the size of the region over which one averages. In particular, in the continuum limit, one finds that $\kappa_{eff} = 6\kappa$ when averaging over one-half of a sphere when fluctuations are ignored. Our results for $\bar{\kappa} = \kappa_{eff}/6$, obtained by averaging over $N_s = (N - 1)/2$ contiguous sites on the vesicle surface, are shown in Fig. 3B (*24*); κ_{eff} is a decreasing function of N for all λ. There does not appear to be any qualitative difference in the behavior of κ_{eff} for large and small λ.

We have not attempted to make a quantitative comparison with theory in the large λ regime, because the expected logarithmic renormalization of κ is completely masked by averaging over a finite portion of the membrane surface (*25*). Nevertheless, the essential qualitative feature that κ_{eff} is a decreasing function of length scale in both the large and small λ regimes supports the interpretation that there is no phase transition as a function of λ.

Self-avoiding fluid membranes are therefore very likely always crumpled at large length scales, independent of the value of the microscopic bending rigidity κ. Furthermore, the crumpled state of the model we considered is a treelike ramified object characterized by $R_g^2 \sim N$, in agreement with results obtained for hypercubic plaquette models (*10*) of random surfaces. A more detailed analysis, however, is required to determine the quantitative scale dependence of the renormalized bending rigidity.

Fluid membranes with a wide range of bare bending rigidities have been studied experimentally in considerable detail recently. For phospholipid bilayers at room temperature, $\kappa/kT \approx 10$ to 20 [see (*26–28*), which contain many additional references], so that the persistence length is usually much greater than the size of the membranes and the reduction of the bending rigidity by shape fluctuations is negligible. An exceptionally small value for ξ_p, however, is obtained for lecithin membranes containing a small amount of bipolar lipid (*26*); this may also be the case for surfactant bilayers that form lamellar and bicontinuous phases (*29*). These systems are therefore well suited for experimental studies of flexible fluid membranes.

We have shown that simulations performed using simple string-and-bead models for randomly triangulated surfaces (with a wide range of finite bare bending rigidities) can yield detailed information on both the large-length-scale conformation as well as the scale dependence of elastic constants such as the bending rigidity. Further numerical studies of this model and its generalizations should permit a more detailed comparison with experiment and could provide new insight into many phenomena involving membranes and other self-assembling structures.

REFERENCES AND NOTES

1. D. R. Nelson, T. Piran, S. Weinberg, Eds., *Statistical Mechanics of Membranes and Surfaces*, (World Scientific, Singapore, 1989).
2. R. Lipowsky, *Nature* **349**, 475 (1991).
3. The precise definition of the lateral tension in fluctuating membranes is a somewhat subtle and often confused issue. See (*4*) for a discussion of this point.
4. F. David and S. Leibler, *J. Phys. II France* **1**, 959 (1991).
5. F. Brochard and J. F. Lennon, *J. Phys.* (*Paris*) **36**, 1035 (1975).
6. P. G. de Gennes and C. Taupin, *J. Chem. Phys.* **86**, 2294 (1982).
7. L. Peliti and S. Leibler, *Phys. Rev. Lett.* **54**, 1690 (1985).
8. D. Forster, *Phys. Lett.* **114A**, 115 (1986); H. Kleinert, *ibid.*, p. 263; *ibid.* **116A**, 57 (1986).
9. We follow the current general usage of the word crumpled to describe a fractal, self-similar object for which all eigenvalues of the moment-of-inertia tensor scale with the same exponent.
10. U. Glaus, *Phys. Rev. Lett.* **56**, 1996 (1986); *J. Stat. Phys.* **50**, 1141 (1988).
11. M. E. Cates, *Phys. Lett.* **161B**, 363 (1985).
12. This definition of ν corresponds to that generally used in studies of tethered membranes. It has also been used in (*2*) and (*13*) to describe the crumpled state of fluid membranes. This definition of ν is twice that used in (*10*).
13. J.-S. Ho and A. Baumgärtner, *Europhys. Lett.* **12**, 295 (1990); A. Baumgärtner and J.-S. Ho, *Phys. Rev. A* **41**, 5747 (1990).
14. J. Ambjørn, B. Duurhuus, J. Fröhlich, *Nucl. Phys. B* **257**, 433 (1985); *ibid.* **275**, 161 (1986).
15. D. V. Boulatov, V. A. Kazakov, I. K. Kostov, A. A. Migdal, *ibid.*, p. 641.
16. A. Billoire and F. David, *ibid.*, p. 617.

17. C. F. Baillie, D. A. Johnston, R. D. Williams, *ibid.* **335**, 469 (1990).
18. This result can be obtained by covering a sphere with equilateral triangles of side ℓ and taking the limit $\ell \to 0$. A similar procedure was followed in (*19*) for a cylindrical surface; in that case it was found that $\kappa = \sqrt{3}\lambda/2$.
19. H. S. Seung and D. R. Nelson, *Phys. Rev. A* **38**, 1005 (1988).
20. Unlike (*13*) (in which the maximum number of nearest-neighbor bonds was limited to eight), we do not explicitly restrict the maximum number of neighbors. We find, for example, that the average maximum connectivity of a monomer is ~12 for the largest systems studied (for $\lambda = 0$). We have checked, however, that restricting the maximum number of nearest neighbors as in (*13*) does not prevent the observed collapse to branched polymer behavior.
21. K. Fujikawa, *Nucl. Phys. B* **226**, 437 (1985).
22. G. Gompper and D. M. Kroll, *J. Phys. I France* **1**, 1411 (1991).
23. C. Itzykson, in *Proceedings of the GIFT Seminar, Jaca 85*, J. Abad *et al.*, Eds. (World Scientific, Singapore, 1986), pp. 130–188.
24. In evaluating $\bar{\kappa}$ we have used $\langle A \rangle \approx 2N_s(1 - 2/N)\langle A_\Delta \rangle$, with $\langle A_\Delta \rangle \approx 0.78$, where $\langle A_\Delta \rangle$ is the average area of an elementary triangle.
25. See (*22*) for a partial treatment of this problem for tethered membranes.
26. H. P. Duwe, J. Käs, E. Sackmann, *J. Phys.* (*Paris*) **51**, 945 (1990).
27. E. Evans and W. Rawicz, *Phys. Rev. Lett.* **64**, 2094 (1990).
28. M. Mutz and W. Helfrich, *J. Phys.* (*Paris*) **51**, 991 (1990).
29. J. M. Di Miglio, M. Dvolaitzky, L. Leger, C. Taupin, *Phys. Rev. Lett.* **54**, 1686 (1985).
30. Supported in part by the University of Minnesota Army High Performance Computing Research Center, U.S. Army contract DAAL03-89-C-0038, NATO grant CRG910156, and the Deutsche Forschungsgemeinschaft through Sonderforschungsbereich 266. D.M.K. has benefited from correspondence with M. E. Fisher and discussions with G. Grest.

30 September 1991; accepted 24 December 1991

Thermal Conductivity of Monolithic Organic Aerogels

X. Lu, M. C. Arduini-Schuster, J. Kuhn, O. Nilsson, J. Fricke, R. W. Pekala

The total thermal conductivity λ of resorcinol-formaldehyde aerogel monoliths has been measured as a function of density ρ in the range from $\rho = 80$ to 300 kilograms per cubic meter. A record-low conductivity value in air at 300 K of $\lambda \approx 0.012$ watt per meter per kelvin was found for $\rho \approx 157$ kilograms per cubic meter. Caloric measurements under variation of gas pressure as well as spectral infrared transmission measurements allowed the determination of solid conductivity, gaseous conductivity, and radiative conductivity as a function of density. The development of such low conductivity materials is of great interest with respect to the substitution of environmentally harmful insulating foams made from chlorofluorocarbons.

Opacified monolithic silica aerogels (*1–3*) have smaller thermal conductivities than all other thermal insulants at ambient conditions (*4*). The reasons include: (i) the high porosity of the SiO_2 skeleton and thus the small solid conductivity (*5*); (ii) the extremely small pore sizes, typically 1 to 100 nm across, that cause a partial suppression of gaseous thermal conductivity (*4*); and (iii) a high specific extinction of thermal radiation if an opacifier (for example, carbon black) is integrated into the SiO_2 skeleton (*4*).

The smallest conductivity value for an opacified SiO_2 aerogel with $\rho = 120$ kg m^{-3} in air was measured to be $\lambda = 0.013$ W m^{-1} K^{-1} (*4*). Such aerogels thus have a large potential for applications in freezers and refrigerators as well as heat storage and transport systems. As nonporous organic materials in general have smaller solid thermal conductivities than nonporous inorganic materials under comparable conditions, we surmised that organic aerogels would provide an even higher thermal resistance than SiO_2 aerogels. In order to verify this assumption we performed caloric measurements on resorcinol-formaldehyde (RF) aerogels. In addition we quantified the radiative heat transfer by determination of the spectral infrared (IR) optical extinction.

These RF aerogels were made by base-catalyzed aqueous polycondensation of resorcinol (1,3-dihydroxybenzene) with formaldehyde (*6, 7*). In this polymerization, resorcinol serves as a trifunctional monomer capable of adding formaldehyde in the 2-, 4-, and 6-ring positions. This monomer is especially reactive because of the attached hydroxyl groups. The substituted resorcinol rings agglomerate to form clusters 3 to 20 nm across in solution. The cluster size is regulated by the concentration of the catalyst (for example, sodium carbonate). The clusters have surface groups, such as $-CH_2OH$, that react further to form a dark red gel. The solution (basically water) in the pores of the RF gel is exchanged with an organic solvent (for example, acetone) and then with CO_2. Supercritical drying with respect to CO_2 (temperature $T \approx 31$°C, critical pressure $p_c \approx 74$ bar) was performed. The resulting RF aerogels show a considerable mechanical flexibility in contrast to their SiO_2 counterparts, which in general are brittle.

Aerogels of RF that are 1 cm thick provide enough IR absorption to be treated as optically thick. Thus radiative transport is a local phenomenon that can be described by the thermal conductivity λ_r:

$$\lambda_r = (16/3)n^2\sigma T_r^3/[e(T_r)\rho] \quad (1)$$

where n is the mean index of refraction of the insulation (for low-density insulations, n is close to 1), σ is the Stefan-Boltzmann constant, T_r is the radiative temperature [calculated from the boundary temperatures T_1 and T_2 (*1*, p. 96) as $T_r^3 = (1/4)(T_1^2 + T_2^2)(T_1 + T_2)$], and the product $e \cdot \rho = E$ is the extinction coefficient, which is equal to $1/l_{photon}$, where l_{photon} is the photon mean free path. In optically thick insulations the photon mean free path is very small compared to the thickness of the specimen. The temperature-dependent specific extinction coefficient $e(T_r)$ is derived from the spectral specific extinction (Fig. 1) by proper spectral averaging (Rosseland mean) (*8*).

The solid conductivity λ_s of monolithic aerogels strongly depends on the density. For silica aerogels, the relation is (*9*)

$$\lambda_s \propto \rho^\alpha, \text{ where } \alpha \approx 1.5 \quad (2)$$

in the density range 70 to 230 kg m^{-3}. The conductivity λ_{evac} for evacuated opacified and thus optically thick aerogels can be approximated by the arithmetic sum of the solid and the radiative conductivity:

$$\lambda_{evac} = \lambda_s + \lambda_r \quad (3)$$

In general λ_s is much less temperature-dependent than λ_r. If the specific extinction shows only a weak temperature dependence, an approximate value for e can thus be derived from the slope of the $\lambda_{evac}(T_r)$ versus T_r^3 curve. The extrapolation $\lambda_{evac}(T_r^3 \to 0)$ yields an estimate for the solid conductivity. As the organic aerogels cannot withstand temperatures above ~80°C, the available temperature range is too small to allow an accurate determination of e. In this case the specific extinction in the IR infrared must be derived from the specific spectral extinction (absorption) with subsequent Rosseland averaging (*8*).

If air or any other gas is introduced into the porous aerogel, the conductivity increases due to the gaseous conductivity as (*10*):

$$\lambda_g = \frac{\lambda_{g0}\Pi}{1 + 2\beta Kn} \quad (4)$$

X. Lu, M. C. Arduni-Schuster, J. Kuhn, O. Nilsson, J. Fricke, Physikalisches Institut, Universität, Am Hubland, D-8700 Würzburg, Germany.
R. W. Pekala, Chemistry and Materials Research Science Department, Lawrence Livermore National Laboratory (LLNL), Livermore, CA 94550.